Experimental Evidence of a Mechanical Coupling between Layers in an Individual Double-Walled Carbon Nanotube

ARTICLE *in* NANO LETTERS · NOVEMBER 2011

Impact Factor: 13.59 · DOI: 10.1021/nl2026234 · Source: PubMed

NANO LETTERS

LETTER

pubs.acs.org/NanoLett

Experimental Evidence of a Mechanical Coupling between Layers in an Individual Double-Walled Carbon Nanotube

D. Levshov,[†,‡,§] T. X. Than,[†,‡,∥] R. Arenal,[⊥,#] V. N. Popov,[▽] R. Parret,[†,‡] M. Paillet,[†,‡] V. Jourdain,[†,‡] A. A. Zahab,[†,‡] T. Michel,[*,†,‡] Yu. I. Yuzyuk,[§] and J.-L. Sauvajol[†,‡]

[†]Université Montpellier 2, Laboratoire Charles Coulomb UMR 5221, F-34095 Montpellier, France

[‡]CNRS, Laboratoire Charles Coulomb UMR 5221, F-34095 Montpellier, France

[§]Faculty of Physics, Southern Federal University, Rostov-on-Don, Russia

[∥]Laboratory of Carbon Nanomaterials, Institute of Materials Science, Vietnamese Academy of Science and Technology, Hanoi, Vietnam

[⊥]Laboratorio de Microscopias Avanzadas (LMA), Instituto de Nanociencia de Aragon (INA), Universidad de Zaragoza, 50018 Zaragoza, Spain

[#]Laboratoire d'Etude des Microstructures, ONERA-CNRS, 92322 Chatillon, France

[▽]Faculty of Physics, University of Sofia, BG-1164 Sofia, Bulgaria

Supporting Information

ABSTRACT: We perform transmission electron microscopy, electron diffraction, and Raman scattering experiments on an individual suspended double-walled carbon nanotube (DWCNT). The first two techniques allow the unambiguous determination of the DWCNT structure: (12,8)@(16,14). However, the low-frequency features in the Raman spectra cannot be connected to the derived layer diameters d by means of the $1/d$ power law, widely used for the diameter dependence of the radial-breathing mode of single-walled nanotubes. We discuss this disagreement in terms of mechanical coupling between the layers of the DWCNT, which results in collective vibrational modes. Theoretical predictions for the breathing-like modes of the DWCNT, originating from the radial-breathing modes of the layers, are in a very good agreement with the observed Raman spectra. Moreover, the mechanical coupling qualitatively explains the observation of Raman lines of breathing-like modes, whenever only one of the layers is in resonance with the laser energy.

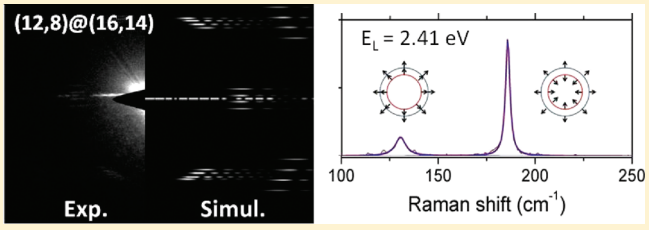

KEYWORDS: Double-walled carbon nanotubes, Raman spectroscopy, breathing-like modes, electron diffraction, transmission electron microscopy

Double-walled carbon nanotubes (DWCNTs) provide the simplest system for studying the interactions between layers in multiwalled carbon nanotubes. Among the different physical interactions, coupled vibrations of the system formed by the inner and outer layers can be studied by Raman spectroscopy. Up to now, mainly the Raman spectra of ensembles of DWCNTs have been measured (see ref 1 and references therein) and only limited information has been derived from isolated DWCNTs.[2−5] Recently, Raman experiments have been performed to study the collective breathing modes in a single individual multiwalled carbon nanotube (MWCNT) characterized by high-resolution transmission electron microscopy (HRTEM).[6] In the latter paper it is concluded that the interlayer coupling in MWCNTs modifies the breathing modes of the individual layers. In the present work, such coupling is evidenced in the case of a DWCNT.

The combination of transmission electron microscopy (TEM), electron diffraction (ED), and resonant Raman spectroscopy on an individual suspended (free-standing) nanostructure is the ultimate method to determine unambiguously the structural parameters, optical transitions, and the Raman-active phonons. This approach has been successfully used to determine the radial breathing mode (RBM) and the G bands features, as well as to evaluate the transition energies of individual, achiral and chiral, semiconducting, and metallic index-identified suspended single-walled carbon nanotubes (SWCNTs)[7−13] and also to identify the Raman fingerprint of graphene.[14] Combined Rayleigh scattering and ED experiments have also allowed determination of the optical transitions of individual index-identified SWCNTs.[15]

In order to study in detail the Raman spectrum of DWCNTs, we follow the same approach as the one developed for SWCNTs.[7] We show that for a complex system such as a DWCNT (more complex than SWCNT) the complementarity of the information provided, on one hand from TEM and electron diffraction and on the other hand from Raman

Received: July 30, 2011
Revised: October 13, 2011
Published: October 18, 2011

experiments, is essential to evidence the coupling between the layers of an individual DWCNT. The observation of this coupling and a better understanding of these vibrations are also important for characterization purposes because Raman spectroscopy is widely used to characterize the structure of carbon nanotubes.

The first signature of mechanical coupling between the two layers of a DWCNT is seen in the low frequency range of the Raman spectrum where the in-phase and the counterphase radial breathing modes of both layers, the so-called breathing-like modes (BLMs), are dominant.[16,17] The mechanical coupling depends on the interlayer distance and diameter. First, for an interlayer distance larger than 0.4 nm, a weak interaction between both layers is expected independently of tube diameter.[16] Assuming an interlayer distance close to 0.34 nm, two coupling regimes were theoretically found as a function of the tube diameter: for outer tube diameters smaller than 2 nm, the vibrations of the inner and the outer tubes are independent. In this weak coupling regime, the in-phase BLM, at low frequency, and the counterphase BLM, at high frequency, tend to the RBM of the outer and inner tubes, respectively. With respect to the RBM of the corresponding SWCNT, only an upshift is expected depending on the interactions between the tubes. On the contrary, in the strong coupling regime, for outer tube diameter larger than 2 nm, the BLMs are collective breathing vibrations of both layers.[16]

The investigated long individual suspended DWCNT was synthesized by chemical vapor deposition (CVD) directly onto a Si_3N_4 TEM grid with holes (2 μm in diameter). The details of the new method used to prepare individual suspended DWCNTs are reported in ref 18.

Resonant Raman scattering measurements were carried out using a Jobin Yvon T64000 spectrometer equipped with a liquid-nitrogen-cooled silicon CCD detector. The scattered light was collected through a 100× objective (N.A. = 0.95) using a back-scattering configuration. In all the measurements, both incident and scattered light polarizations are along the nanotube axis (∥ ∥ polarized Raman spectrum). Incident excitations from Ar^+ and Kr^+ lasers were used: 488 nm (2.54 eV), 514.5 nm (2.41 eV), 568.1 nm (2.18 eV), and 647.1 nm (1.92 eV). In order to avoid heating effects, the laser power impinging the sample was kept below 50 μW.

TEM images and ED patterns were recorded in a FEI Titan microscope operating at 80 kV and within short acquisition times (less than 5 s for ED) to reduce damage induced by electron irradiation.

Figure 1 shows the investigated DWNT placed across holes of the grid. This configuration minimizes the effects (upshift of the Raman modes and downshift of the optical transitions) caused by tube−tube interactions within a rope, tube−substrate interactions for tubes deposited on a substrate, and tube−surfactant interactions in measurements on ensembles of DWCNTs wrapped in surfactant. The structural data derived from TEM and ED for the DWCNT (Figure 1) can be summarized as follows: the nanotube is longer than 30 μm (Figure 1a). The HRTEM image (Figure 1b) clearly allows one to identify this tube as a DWCNT and shows the presence of a certain quantity of amorphous carbon on its surface. TEM measurements at different holes of the grid also confirm that the structure of the tube is conserved along its length. Due to the vibration of the nanotube under the electron beam, it was impossible to derive the diameter of each layer with a good accuracy from the HRTEM image. Moreover, we note that the HRTEM technique is very sensitive to the orientation of the tube with respect to the electron beam and

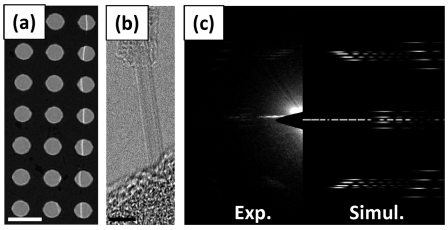

Figure 1. (a) Low magnification TEM image of the suspended nanotube on the Si_3N_4 grid, the scale bar is 4 μm. (b) HRTEM of the same DWCNT, the scale bar is 3 nm. (c) Experimental (left) and simulated (right) diffraction pattern of the (12,8)@(16,14) DWCNT.

to the defocus conditions.[19] Therefore, the atomic structure of a nanotube can be obtained by HRTEM only under particular observation conditions, which limits the use of this technique for such studies.[20] Electron diffraction does not have these limiting factors and is therefore the most reliable technique to obtain the nanotube's atomic structure.

The ED patterns contain structural information about the DWCNT. First, the diameters of the two layers can be derived from the equatorial line analysis. The equatorial line oscillates with two periods related to the average radius of the DWCNT for the shorter period and to the interlayer distance for the higher period.[21] Unfortunately, the latter information is not available with a good accuracy in our case due to the presence of the beam stop which masks the equatorial line on one side of the diffraction pattern. Consequently, the value obtained for the average diameter is found to be 1.9 nm with an error bar estimated at 10%. The second information concerns the chiral angles. They are derived from the two pairs of hexagons which appear on the diffraction pattern (layer-lines). First, the appearance of two pairs of hexagons immediately rules out the presence of an achiral layer in the DWCNT. The analysis of the layer-lines, using a procedure which takes into account the distances between the different layers,[22,23] provides accurate information about the chiral angle of each layer. The derived values are 23.4° and 27.7°, with an error bar of ±0.2°. Considering these values as a starting point for the indexation of the DWCNT, we compute all the possible (n,m) tubes that have chiral angles of 23.4° and 27.7° within the error bars. For $d \leq 2.5$ nm, this leads to six possibilities for chiral angles $(23.4 \pm 0.2)°$ and four possible indices for chiral angles $(27.7 \pm 0.2)°$, giving 24 different indices for the DWCNT. Keeping in mind that the difference of the two diameters in a DWCNT should be close to 0.68 nm, only two pairs of indices are possible: (8,7)@(15,10) and (12,8)@(16,14). The former DWCNT can be ruled out because it disagrees with the average diameter derived from the equatorial line analysis. Moreover, using the recently developed technique by Deniz et al. for the analysis of the ED patterns of multiwalled nanotubes,[24] we conclude that the investigated tube corresponds to (12,8)@(16,14). Furthermore, this identification of the atomic structure is confirmed by the comparison of the experimental and the simulated ED pattern, as displayed in Figure 1c. The diameters of these chiral nanotubes are respectively d_{in} = 1.36 nm and d_{out} = 2.03 nm in agreement with the estimation provided by the HRTEM images. We note that each layer of this DWCNT is semiconducting, the inner being of type I $(\mathrm{mod}(n - m;3) = 1)$ and the outer being of type II $(\mathrm{mod}(n - m;3)=2)$.

Figure 2 displays the low frequency region of the Raman spectra of the (12,8)@(16,14) DWCNT for different laser

dx.doi.org/10.1021/nl2026234 |Nano Lett. 2011, 11, 4800–4804

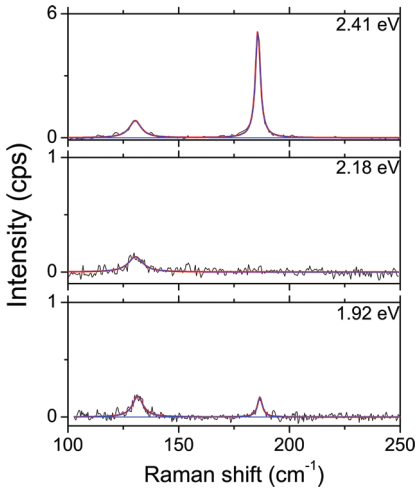

Figure 2. Low frequency range of the Raman spectra of the (12,8)@(16,14) DWCNT measured at three excitation energies (for top to bottom: 2.41, 2.18, 1.92 eV).

Table 1. Calculated RBM Frequencies from Two Different Relations $\omega_{RBM,1}(d) = 228/d$ (nm) and $\omega_{RBM,2}(d) = 204/d$ (nm)) + 27 (see text)

(n,m)	d, nm	$\omega_{BLM,exp}$, cm^{-1}	$\omega_{RBM,2}(d)$, cm^{-1}	$\omega_{RBM,1}(d)$, cm^{-1}
(12,8)	1.36	186	177	167.5
(16,14)	2.03	133	127.5	112.5

excitation energies E_L. At E_L = 2.41 eV (Figure 2, top), two strong components are observed at 133 cm^{-1} (full width at half-maximum, fwhm = 6.5 cm^{-1}) and 186 cm^{-1} (fwhm = 3 cm^{-1}), respectively. At E_L = 2.18 eV, only the component at 133 cm^{-1} is observed with a very low intensity. Finally, the two peaks are retrieved at almost the same frequencies and fwhm when the excitation is tuned at 1.92 eV. At this energy, the fwhm are also comparable to those observed at 2.41 eV, i.e., 6 cm^{-1} for the low frequency peak and 3 cm^{-1} for the high frequency peak.

Normally, the diameters of the inner and outer tubes are derived from the BLM frequencies using ω_{RBM} vs d established for SWCNTs.[2] The frequency of the counterphase BLM measured on the (12,8)@(16,14) DWCNT can be compared to that of the RBM measured on the (12,8) SWCNT.[10] The RBM frequency of the (12,8) SWCNT is located at 174.6 cm^{-1}, downshifted by about 11 cm^{-1} with respect to the counterphase BLM of the DWCNT. This shift is a clear signature of interlayer interaction. More generally, the experimental frequencies of both BLMs can be compared to those predicted from the ω_{RBM} vs d relationships derived from experiments on suspended individual SWCNTs. For individual suspended index-identified SWCNTs in air, two different relations were proposed, namely, $\omega_{RBM,1}(d) = 228/d$ (nm) for tubes free of any environment (except air)[13] and $\omega_{RBM,2}(d) = 204/d$ (nm) + 27.[7] The difference between the two relations is tentatively assigned to the presence of amorphous carbon around the tubes. All other empirical relations proposed for individual SWNTs wrapped in a surfactant give values between $\omega_{RBM,1}(d)$ and $\omega_{RBM,2}(d)$. The RBM frequencies of the (12,8) and (16,14) individual SWCNTs evaluated from the latter relations are given in Table 1.

Both relations $\omega_{RBM}(d)$ underestimate the frequencies of the BLMs (Table 1). Considering the $\omega_{RBM,1}(d)$ relation, the interaction between the layers upshifts by 20 cm^{-1} the in-phase and counterphase BLM. On the other hand, by considering the relation $\omega_{RBM,2}(d)$, an upshift of about 5 cm^{-1} (respectively 9 cm^{-1}) for the in-phase (respectively counterphase) BLM is found. A precise description of the role of the coupling between the tubes, especially as a function of the tube diameters and interlayer distance, requires additional measurements on several index-identified DWCNTs. An important result is that all $\omega_{RBM}(d)$ relations established for SWCNTs do not work for this DWCNT.

The Raman data can be compared to the predictions of a theoretical model for calculation of phonons in DWCNT,[16,17] in particular concerning the diameter dependence of the BLMs. In this context, we use the theoretical predictions of ref 16. In this model, the shift of the BLMs with respect to the RBM frequency of the individual inner and outer layers (given by $\omega_{RBM}(d) = 228/d$ (nm) for each independent layer), is calculated by taking into account the van der Waals interactions between the layers. According to Figure 4 of ref 16, the mode at 186 cm^{-1} corresponds to a diameter of the outer tube close to 2.02 nm in very good agreement with the diameter of the (16,14). From the same figure, the in-phase mode is predicted at 123 cm^{-1}, lower than the measured one. A better agreement with experiment is achieved by calculating the shift of the frequencies of the BLMs with respect to the frequency of the RBMs by considering two different relations for the RBM frequency of each independent layer, namely, $\omega_{RBM}(d) = 228/d$ (nm) for the inner tube and $\omega_{RBM}(d) = 204/d$ (nm) + 27 for the outer tube. The presence of amorphous carbon around the outer tube justifies to consider such a relation. With this assumption, for an outer tube diameter of 2.02 nm, the frequency of the counterphase mode frequency is calculated at 186 cm^{-1} and that of the in-phase mode around 136 cm^{-1}, in better agreement with the experimental values.

The major drawback of measurements on a single suspended index-identified carbon nanotube is probably the difficulty to obtain statistical information. However this approach is the only one that permits information to be obtained about the G band. In the $\parallel\parallel$ configuration, two modes with A_1 symmetry are expected to be Raman active for semiconducting chiral SWCNTs. Therefore, the G band displays two components: G^- and G^+ associated with the TO and LO phonons, respectively. Figure 3 shows the G band measured on the (12,8)@(16,14) DWCNT at different laser excitation energies. At 2.54 eV, where no BLM is observed, a strong G band signal is detected because at this energy the nanotube is in resonance with the outgoing light scattered by the G modes. We note that only a single G^- band is observed at this energy. At 2.41 and 2.18 eV, the G band is composed of three components located at 1590, 1570, and 1564.5 cm^{-1}, the latter being very weak at 2.18 eV. Finally, at 1.92 eV only the G^+ band at 1589 cm^{-1} is detected with a small component around 1570 cm^{-1}. With respect to the G modes measured on semiconducting SWCNTs, it is reasonable to assign the components at 1570 and 1564.5 cm^{-1} to the TO modes of the outer and inner tube, respectively, and consider the G^+ band as a superposition of the LO modes of both tubes. These conclusions are based on the following considerations: (i) The diameter dependence of the TO phonon modes in semiconducting SWCNTs has been measured[8] and well-described theoretically (see, e.g., ref 26). For SWCNT with diameters ≈1.3 and ≈2.0 nm, the TO modes appear at ≈1565 and ≈1573 cm^{-1}, respectively. In ref 10, the TO component directly measured on the (12,8) SWCNT was reported at 1562.5 cm^{-1}. These frequencies are close to the G^-

dx.doi.org/10.1021/nl2026234 |Nano Lett. 2011, 11, 4800–4804

components measured on the DWCNT. (ii) For SWCNTs with diameter ≥1.4 nm, the frequency of the LO phonon is measured at about 1590 cm^{-1}, independently of the diameter. This explains why no splitting of the LO bands coming from the inner and the outer tube is observed in the investigated DWCNT. Then taking the results for SWCNTs as a reference, by contrast to RBMs, no significant shift of the G modes due to the interaction between the layers is measured in the (12,8)@(16,14) DWCNT.

To understand all these results, we use, as commonly done in the literature for individual MWCNTs,[6,2] the Kataura plot calculated for SWCNTs within a nonorthogonal tight-binding model (NTB)[29] and corrected with a rigid upshift to agree with the transitions measured on well identified SWCNTs.[9] The use of such a Kataura plot is validated by the fact that measurements

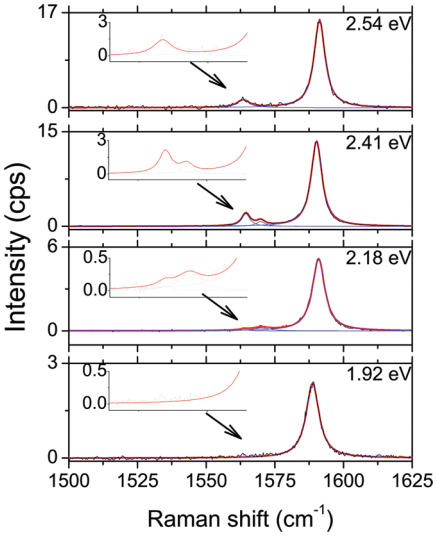

Figure 3. G band of the (12,8)@(16,14) DWCNT measured at four excitation energies (from top to bottom: 2.54, 2.41, 2.18, 1.92 eV). Inset: zoom of the G^- band in the 1550−1585 cm^{-1} frequency range. The spectra are fitted with Lorentzian.

of the transition energies on DWCNTs only display slight shift with respect to the transition energies in the corresponding SWCNTs.[27,28] The Kataura plot is represented in Figure 4 and the transition energies for the third and fourth semiconducting transitions of the corresponding (12,8) and (16,14) SWCNTs are denoted by gray dots. It must be pointed out that the diameters of the inner and outer layers (indicated by vertical gray lines in Figure 4) cannot be derived from any RBM versus diameter relation but are obtained by ED as discussed previously.

At 2.54 eV, no transition is expected for the two tubes, which explains why no BLM is detected. At 2.41 eV, the laser energy is very close to the E_{33} transition (2.43 eV) expected for the (12,8) inner tube. By contrast no transition is expected at this energy for the (16,14) outer tube. It must be emphasized that the incoming resonance of the inner tube at 2.41 eV explains the observation of G modes of the inner tube at 2.54 eV (outgoing resonance). At 2.18 eV, the laser energy is close to the E_{44} = 2.17 eV transition energy of the (16,14) outer nanotube. Finally, at 1.92 eV the difference with the E_{33} = 1.85 eV of the (16,14) is small enough to assume that the outer tube is in incoming resonance at this energy.

The examination of the resonance conditions for the investigated DWCNT on the basis of the Kataura plot yields conclusions that disagree with experiment. Indeed, at 2.41 and 1.92 eV excitation energies, only one tube of the DWCNT is in resonance though we measure two distinct BLMs. The disagreement is resolved by considering a mechanical coupling between the two layers. In that case, only the optical resonance of one tube is necessary to observe the response of the coupled system.[30] This mechanical coupling has already been reported for individual bundles[12] and, for the first time, is directly evidenced in the case of a DWCNT. Qualitatively, if one layer is in resonance, the coupling can induce the observation of all BLMs of the DWCNT and a relatively small intensity of the mode assigned to the nonresonant layer is expected. To take into account the coupling between the layers is the only way to explain coherently the majority of the present results. Nevertheless, this coupling does not explain the absence of the counterphase mode at 2.18 eV (Figure 2). We emphasize that the use of the Kataura plot to

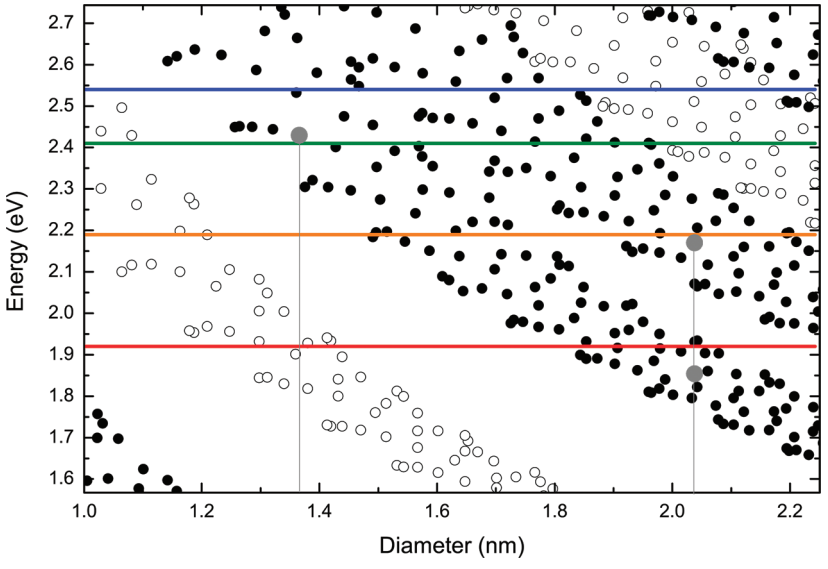

Figure 4. Normalized Kataura plot: open (black) symbols, transition energies for metallic (semiconducting) SWCNTs; gray symbols, transitions for the (12,8) and (16,14) SWCNTs; horizontal lines, laser excitation energies used in this work.

dx.doi.org/10.1021/nl2026234 |*Nano Lett.* 2011, 11, 4800–4804

identify the structure of each layer in a DWCNT by means of the resonance energy and the BLM frequencies is not straightforward.

In conclusion, we presented a detailed Raman study of an individual suspended index-identified DWCNT. The independent structural identification of the investigated DWCNT allowed us to compare the Raman results to previous experimental data and theoretical predictions. We showed that the Raman features obtained at different excitation energies on the (12,8)@(16,14) DWCNT can only be understood in a coherent way by considering the coupling between the two concentric layers. This coupling plays a major role for the conditions for observation of the modes in a Raman spectrum excited at a given laser energy as well as for the frequencies of the in-phase and counterphase BLMs. In terms of characterization, we can conclude that the identification of the indexes of the layers in a DWCNT from the Raman spectra should be done by considering a possible mechanical coupling between the layers.

■ ASSOCIATED CONTENT

Supporting Information. BLM range of Raman spectra of two individual DWCNTs and normalized Kataura plot used to determine the resonance conditions of BLM. This material is available free of charge via the Internet at http://pubs.acs.org.

■ AUTHOR INFORMATION

Corresponding Author
*E-mail: thierry.michel@univ-montp2.fr.

■ ACKNOWLEDGMENT

This work has been done in the framework of the GDR-E No 2756 "Science and Application of the Nanotubes-NANO-E". The authors acknowledge financial support from ANR Excitubes, TRAIN^2 network, and French Russian PICS No. 4818. V.N.P. acknowledges financial support from University of Montpellier 2.

■ REFERENCES

(1) Pfeiffer, R.; Pichler, T.; Kim, Y. A.; Kuzmany, H. In *Carbon Nanotubes: Advanced Topics in the Synthesis, Structure, Properties, and Applications*; Jorio, A., Dresselhaus, G., Dresselhaus, M. S., Eds.; Springer-Verlag: Berlin, 2008; Vol. 111, pp 495−530.

(2) Villalpando-Paez, F.; Son, H.; Nezich, D.; Hsieh, Y. P.; Kong, J.; Kim, Y. A.; Shimamoto, D.; Muramatsu, H.; Hayashi, T.; Endo, M.; Terrones, M.; Dresselhaus, M. S. *Nano Lett.* **2008**, *8* (11), 3879–3886.

(3) Bouilly, D.; Cabana, J.; Meunier, F.; Desjardins-Carrière, M.; Lapointe, F.; Gagnon, P.; Larouche, F. L.; Adam, E.; Paillet, M.; Martel, R. *ACS Nano* **2011**, *5* (6), 4927–4934.

(4) Liu, K. H.; Wang, W. L.; Xu, Z.; Bai, X. D.; Wang, E. G.; Yao, Y. G.; Zhang, J.; Liu, Z. F. *J. Am. Chem. Soc.* **2009**, *131*, 62–63.

(5) Puech, P.; Nanot, S.; Raquet, B.; Broto, J.-M.; Millot, M.; Anwar, A. W.; Flahaut, E.; Bacsa, W. *Phys. Status Solidi B* **2011**, *248* (4), 974–979.

(6) Spudat, C.; Muller, M.; Houben, L.; Maultzsch, J.; Goss, K.; Thomsen, C.; Schneider, C. M.; Meyer, C. *Nano Lett.* **2010**, *10*, 4470–4474.

(7) Meyer, J. C.; Paillet, M.; Michel, T.; Moréac, A.; Neumann, A.; Duesberg, G. S.; Roth, S.; Sauvajol, J.-L. *Phys. Rev. Lett.* **2005**, *95*, 217401.

(8) Paillet, M.; Michel, T.; Meyer, J. C.; Popov, V. N.; Henrard, L.; Roth, S.; Sauvajol, J.-L. *Phys. Rev. Lett.* **2006**, *96*, 257401.

(9) Michel, T.; Paillet, M.; Meyer, J. C.; Popov, V. N.; Henrard, L.; Sauvajol, J.-L. *Phys. Rev. B* **2007**, *75*, 155432.

(10) Michel, T.; Paillet, M.; Nakabayashi, D.; Picher, M.; Jourdain, V.; Meyer, J. C.; Zahab, A. A.; Sauvajol, J.-L. *Phys. Rev. B* **2009**, *80*, 245416.

(11) Michel, T.; Paillet, M.; Meyer, J. C.; Popov, V. N.; Henrard, L.; Poncharal, P.; Zahab, A.; Sauvajol, J.-L. *Phys. Status Solidi B* **2007**, *244*, 3986–3991.

(12) Débarre, A.; Kobylko, M.; Bonnot, A. M.; Richard, A.; Popov, V. N.; Henrard, L.; Kociak, M. *Phys. Rev. Lett.* **2008**, *101*, 197403.

(13) Liu, K.; Wang, W.; Wu, M.; Xiao, F.; Hong, X.; Aloni, S.; Bai, X.; Wang, E.; Wang, F. *Phys. Rev. B* **2011**, *83*, 113404.

(14) Ferrari, A. C.; Meyer, J. C.; Scardaci, V.; Casiraghi, C.; Lazzeri, M.; Mauri, F.; Piscanec, S.; Jiang, D.; Novoselov, K. S.; Roth, S.; Geim, A. K. *Phys. Rev. Lett.* **2006**, *97*, 187401.

(15) Sfeir, M. Y.; Beetz, T.; Wang, F.; Huang, L.; Huang, X. M. H.; Huang, M.; Hone, J.; O'Brien, S.; Misewich, J. A.; Heinz, T. F.; Wu, L.; Zhu, Y.; Brus, L. E. *Science* **2006**, *312*, 554–556.

(16) Popov, V. N.; Henrard, L. *Phys. Rev. B* **2002**, *65*, 235415.

(17) Rahmani, A.; Sauvajol, J.-L.; Cambedouzou, J.; Benoit, C. *Phys. Rev. B* **2005**, *71*, 125402.

(18) Tinh, T. X.; Nguyen, V. C.; Jourdain, V.; Paillet, M.; Kim, D.-Y.; Sauvajol, J.-L.; Ngo, T. T. T.; Phan, N. M. *J. Exp. Nanosci.* **2011**, *6*, 1–10.

(19) Qin, C.; Peng, L.-M. *Phys. Rev. B* **2002**, *65*, 155431.

(20) Arenal, R.; Blase, X.; Loiseau, A. *Adv. Phys.* **2010**, *59*, 101.

(21) Kociak, M.; Hirahara, K.; Suenaga, K.; Iijima, S. *Eur. Phys. J. B* **2003**, *32*, 457–469.

(22) Gao, M.; Zuo, J. M.; Twesten, R. D.; Petrov, I.; Nagahara, L. A.; Zhang, R. *Appl. Phys. Lett.* **2003**, *82*, 2703.

(23) Arenal, R.; Kociak, M.; Loiseau, A.; Miller, D.-J. *Appl. Phys. Lett.* **2006**, *89*, 073104.

(24) Hakan, D.; Anna, D.; Lu-Chang, Q. *Ultramicroscopy* **2010**, *111*, 66–72.

(25) Mahan, G. D. *Phys. Rev. B* **2002**, *65*, 235402.

(26) Popov, V. N.; Lambin, P. *Phys. Rev. B* **2006**, *73*, 085407.

(27) Villalpando-Paez, F.; Moura, L. G.; Fantini, C.; Muramatsu, H.; Hayashi, T.; Kim, Y. A.; Endo, M.; Terrones, M.; Pimenta, M. A.; Dresselhaus, M. S. *Phys. Rev. B* **2010**, *82*, 155416.

(28) Hertel, T.; Hagen, A.; Talalaev, V.; Arnold, K.; Hennrich, F.; Kappes, M.; Rosenthal, S.; McBride, J.; Ulbricht, H.; Flahaut, E. *Nano Lett.* **2005**, *5* (3), 511–514.

(29) Popov, V. N.; Henrard, L. *Phys. Rev. B* **2004**, *70*, 115407.

(30) The same behavior is shown on two nonindex-identified DWCNTs, see Supporting Information.